

Article

Effect of Al Content on Phase Compositions of FeNiCoCrMo_{0.5}Al_x High Entropy Alloy

Anton Semikolenov ^{1,2}, Svetlana Shalnova ², Victor Klinkov ^{1,*}, Valentina Andreeva ¹, Maria Salynova ¹, Tatiana Larionova ¹ and Oleg Tolochko ¹ 

- ¹ Institute of Mechanical Engineering, Materials and Transport, Peter the Great St. Petersburg Polytechnic University (SPbPU), Polytechnicheskaya 29, 195251 St. Petersburg, Russia; semikolenov.a@edu.spbstu.ru (A.S.); andreeva_vd@spbstu.ru (V.A.); salynova_ma@spbstu.ru (M.S.); larionova_TV@spbstu.ru (T.L.); tolochko_ov@spbstu.ru (O.T.)
- ² Institute of Laser and Welding Technologies, State Marine Technical University, Lotsmanskaya Ulitsa, 10, 190121 St. Petersburg, Russia; s.shalnova@corp.smtu.ru
- * Correspondence: klinkov_va@spbstu.ru

Abstract: The FeCoNiCrMo_{0.5}Al_x system with x up to 2.13 was analyzed from the point of view of evolution of the phase composition and microstructure. Cast samples were synthesized by induction melting and analyzed by X-ray diffraction, energy dispersive spectroscopy, scanning electron microscopy, and Vickers microhardness test methods. Phase compositions of these alloys in dependence on Al concentration consist of FCC solid solution, σ -phase, NiAl-based B2 phase, and BCC solid solution enriched with Mo and Cr. Phase formation principles were studied. Al dissolves in a FeCoNiCrMo_{0.5} FCC solid solution up to 8 at.%; at higher concentrations, Al attracts Ni, removing it from FCC solid solution and forming the B2 phase. Despite Al not participating in σ -phase formation, an increase in Al concentration to about 20 at.% leads to a growth in the σ -phase fraction. The increase in the σ -phase was caused by an increase in the amount of B2 because the solubility of σ -forming Mo and Cr in B2 was less than that in the FCC solution. A further increase in Al concentration led to an excess of Mo and Cr in the solution, which formed a disordered BCC solid solution. The hardness of the alloys attained the maximum of 630 HV at 22 and 32 at.% Al.

Keywords: high entropy alloys; σ -phase; XRD; phase composition; microstructure; hardness



Citation: Semikolenov, A.; Shalnova, S.; Klinkov, V.; Andreeva, V.; Salynova, M.; Larionova, T.; Tolochko, O. Effect of Al Content on Phase Compositions of FeNiCoCrMo_{0.5}Al_x High Entropy Alloy. *Metals* **2021**, *11*, 1734. <https://doi.org/10.3390/met11111734>

Academic Editor: Alexander Kauffmann

Received: 29 September 2021

Accepted: 22 October 2021

Published: 29 October 2021

Publisher's Note: MDPI stays neutral with regard to jurisdictional claims in published maps and institutional affiliations.



Copyright: © 2021 by the authors. Licensee MDPI, Basel, Switzerland. This article is an open access article distributed under the terms and conditions of the Creative Commons Attribution (CC BY) license (<https://creativecommons.org/licenses/by/4.0/>).

1. Introduction

The concept of high-entropy alloys (HEA) arose in 2004. It was initiated by the works of Cantor et al. [1] and Yeh et al. [2]. In the former [1], there was a single-phase five component Fe₂₀Cr₂₀Mn₂₀Ni₂₀Co₂₀ alloy reported [1], after that, this composition was named the Cantor alloy. In the latter [2], the idea of high entropy stabilization of multi-principal solid solution was proposed, and the term “high-entropy alloys” was introduced. It was postulated that high entropy promotes the formation of disordered substitutional solid solutions instead of intermetallic phases due to a decrease in free energy. Later in [3,4], based on the experimental data, other criteria of multicomponent solid-solution stabilization have been proposed, namely, atomic-size difference (δ), which should not be higher than 6.6%; mixing enthalpy of solid solution (ΔH_{mix}), which should be in the range of -15 – 5 kJ/mol; and Ω , defined as $T_m \Delta S_{\text{mix}} / |\Delta H_{\text{mix}}|$, which should be ≥ 1.1 . However, these values are based on back-tested correlations, and have little evidence of predictive capability [5]. The unique features attributed to HEA such as solid solution strengthening due to severe lattice-distortion, sluggish diffusion, and the cocktail effect [5–7], were supposed to be caused by the multiprincipal solid solution effect, so in this context, the term HEA should refer to single-phase multiprincipal alloys [8]. However, the majority of HEA considered nowadays in the equilibrium state at an ambient temperature has several phases [9–25], even those that were considered to be single-phase in early

research [16,17]. It is likely that during solidification, the different atoms distribute in accordance with their affinity, leading to liquation, namely, the appearance of regions of different compositions not satisfying the criteria of solid solution formation. On the other hand, when the temperature is lowered, the effect of entropy decreases, so the solid solution tends to decompose or order, but due to sluggish diffusion, these processes may go slowly, and so are not completed at ambient conditions [8,17]. Precipitation behavior in HEA is complex and abstruse and may induce the formation of useful properties as well as their deterioration and instability. Currently, methods are being developed to predict the formation and stability of HEA taking into account the formation enthalpies of competing phases [13,26]. To date, among all the others that ever proposed HEA, the alloys based on an AlCoCrFeNi system have been the most studied [2,5,9–15,19–25]. The reason for this are the outstanding mechanical properties and phase formation phenomena. In AlCoCrFeNi alloys, Al has the largest impact on the structure: a crystal structure transforms from FCC to BCC as the Al content increases [2]. In [27], an effect of valence electron concentration (VEC) on the stability of FCC and BCC solid solutions was demonstrated: the FCC solid solution was found to be stable at higher VEC and instead, BCC phase is stable at lower VEC (<6.87). In [28], the effect of Al on the crystal structures was analyzed using first-principles electronic structure calculations. It was demonstrated that due to strongly attractive interactions between Al and other elements, partially disordered structures (L12, DO3, and B2) became more stable than the disordered solid solutions. As a result, the elements segregate, forming Ni-Al-rich and Fe-Cr-rich areas [9,13,15,22]. Cr and Fe stabilize the BCC structure [11,12,28], while Ni and Co stabilize the FCC solid solution [10,22,28]. Compared to disordered solid solutions, ordered BCC (B2) compounds based on NiAl have a unique set of strength characteristics at elevated and high temperatures, and their strength practically does not degrade up to temperatures of 800–900 °C [29]. The high hardness of AlCrFeCoNi and AlCrFeCoNiTi alloys was attributed namely to the formation of the NiAl-B2 phase [19,20]. Partially disordered NiAl-based B2 alloys with refractory metals may be considered as promising structural materials for high-temperature applications [29]. An addition of Nb to AlCoCrFeNi studied in [30] results in the formation of a Laves phase of the (CoCr)Nb type and BCC solid solution and an increase in strength and hardness. An effect of V addition was studied in [31] and it was found that V addition reduces element segregation and homogenizes the microstructure. An addition of Mo significantly increased the strength and thermal stability of CoCrFeNiMo alloys, and the effect was caused by the σ or σ and μ phase formation [32,33]. The σ -phase occurs in the majority of transition-metal alloys [16,17,21,23,33–36]. It is a hard and brittle topologically close packed phase, and its appearance in stainless steels usually results in the deterioration of the properties due to brittleness and the removal of Cr from the solid solution matrix [35,36].

In this work, the Al_xFeCoNiCrMo system was analyzed from the point of view of the evolution of phase composition and microstructure. Mo is a refractory metal and is added to AlCoCrFeNi with the aim to increase alloy strength and thermal stability, however, it is known to be a strong promoter of the σ -phase. Al, in contrast, suppresses σ -phase formation, and tends to form an ordered NiAl-based B2 structure with high strength characteristics at elevated and high temperatures. Thus, Al_xFeCoNiCrMo HEA may be considered as promising structural materials for high-temperature applications, and understanding of the phase formation principles and structure stability in this system is necessary for the development of further alloys. The aim of the study was to observe and analyze the effect of Al concentration on the crystal structure of HEA containing Mo.

2. Materials and Methods

A series of multicomponent alloys of the FeNiCoCrMo_{0.5}Al_x system with x varying from 0 to 2.13 (0–32 at.% Al) were melted in a high-frequency induction furnace in quartz crucibles under an argon atmosphere. Elemental components with a purity of 99.93% or greater were used. The induction melting process took about 2 min, then the samples were cooled in water. Melting of refractory elements occurred via their gradual dissolution in the

melt. For homogenization of the melts, the alloys were remelted three times. The prepared ingots were approximately 30 g. The designation of the samples and the exact composition of the ingots are presented in Table 1.

Table 1. Chemical composition and designation of the FeNiCoCrMo_{0.5}Al_x alloys.

Alloy Designation	Atomic Concentration, %						ΔH_{mix} (kJmol ⁻¹)	ΔS_{mix} (JK ⁻¹ mol ⁻¹)	δ (%)	VEC
	Fe	Ni	Co	Cr	Mo	Al				
Al0 ($x = 0$)	21.98	21.97	21.84	22.22	11.99	-	-4.39	13.18	3.63	7.97
Al4 ($x = 0.18$)	21.24	21.35	21.15	20.82	11.62	3.82	-6.14	14.03	4.32	7.799
Al8 ($x = 0.42$)	20.09	20.16	20.01	20.33	10.98	8.42	-8.04	14.47	4.93	7.555
Al12 ($x = 0.64$)	19.22	19.31	19.15	19.38	10.53	12.41	-9.42	14.64	5.35	7.359
Al16 ($x = 0.91$)	18.40	18.45	18.32	18.17	10.07	16.69	-10.98	14.74	5.71	7.161
Al22 ($x = 1.29$)	17.21	17.28	17.14	16.86	9.43	22.08	-12.47	14.67	6.06	6.887
Al25 ($x = 1.52$)	16.56	16.54	16.55	16.55	8.65	25.15	-13.2	14.54	6.21	6.735
Al29 ($x = 1.84$)	15.71	15.68	15.73	15.7	8.26	28.92	-14.0	14.34	6.37	6.546
Al32 ($x = 2.13$)	14.98	15.03	14.99	15.01	8.04	31.95	-14.43	14.17	6.44	6.392

Scanning electron microscopy (SEM) and energy dispersion spectroscopy (EDS) were performed on using a MIRA 3 microscope (TESCAN, Brno-Kohoutovice Czech Republic). In order to determine the volume fraction of the structural components, the images of the microstructures were analyzed with the software THIXOMET (THIXOMET Pro, Thixomet, Saint-Petersburg, Russia).

The phase composition was examined with a D8 Advance diffractometer (BRUKER, Billerica, MA, USA) under Cu Ka radiation. The solid solution lattice parameter was determined based on the XRD patterns, which were collected in the 2Θ range from 20° to 140° with a speed of $2^\circ/\text{min}$. In order to eliminate the systematic error, the definition of the lattice parameter was calculated using the Nelson–Riley extrapolation function [36]. For convenience, we calculated the shortest interatom distance for each cubic lattice using the lattice parameters determined by XRD. The shortest interatomic distance for FCC was $\frac{1}{2}$ [110] and $\frac{1}{2}$ [111] for BCC. Quantitative phase analysis was fulfilled using DIFFRAC.EVA software (DIFFRAC.EVA V6, BRUKER, Billerica, MA, USA).

Vickers microhardness was tested with a Micromet 5103 (BUEHLER, Lake Bluff, IL, USA) under a load of 1 N and with a dwelling time of 10 s, at least six measurements per point were made. The density of the samples was determined by hydrostatic weighing at a water temperature of 24°C .

3. Results

3.1. Phase Compositions (XRD Results)

Figure 1 demonstrates the XRD patterns of the samples. FCC, BCC solid solutions, B2, and σ -phase were determined. Al4 consists of an incoherent FCC solid solution and σ -phase. In Al8, the peaks of FCC shifted left as evidence of its lattice parameter increase due to a dissolution of Al. Apart from this, in Al12, a peak belonging to the BCC may be observed. Further increase in Al concentration in the alloys (Al25–Al32) led to a total disappearance of the reflexes belonging to the FCC phase and a development of BCC reflexes; besides, a peak at $2\Theta = 32^\circ$ denoting the BCC solution ordering becomes pronounced. In the alloys with an Al concentration higher than 25 at.% (Al25), there were two sets of reflexes of BCC structures observed and intervals between the peaks belonging to each phase increase with an increase in Al concentration in the alloys. The found phases for each alloy are listed in Table 2.

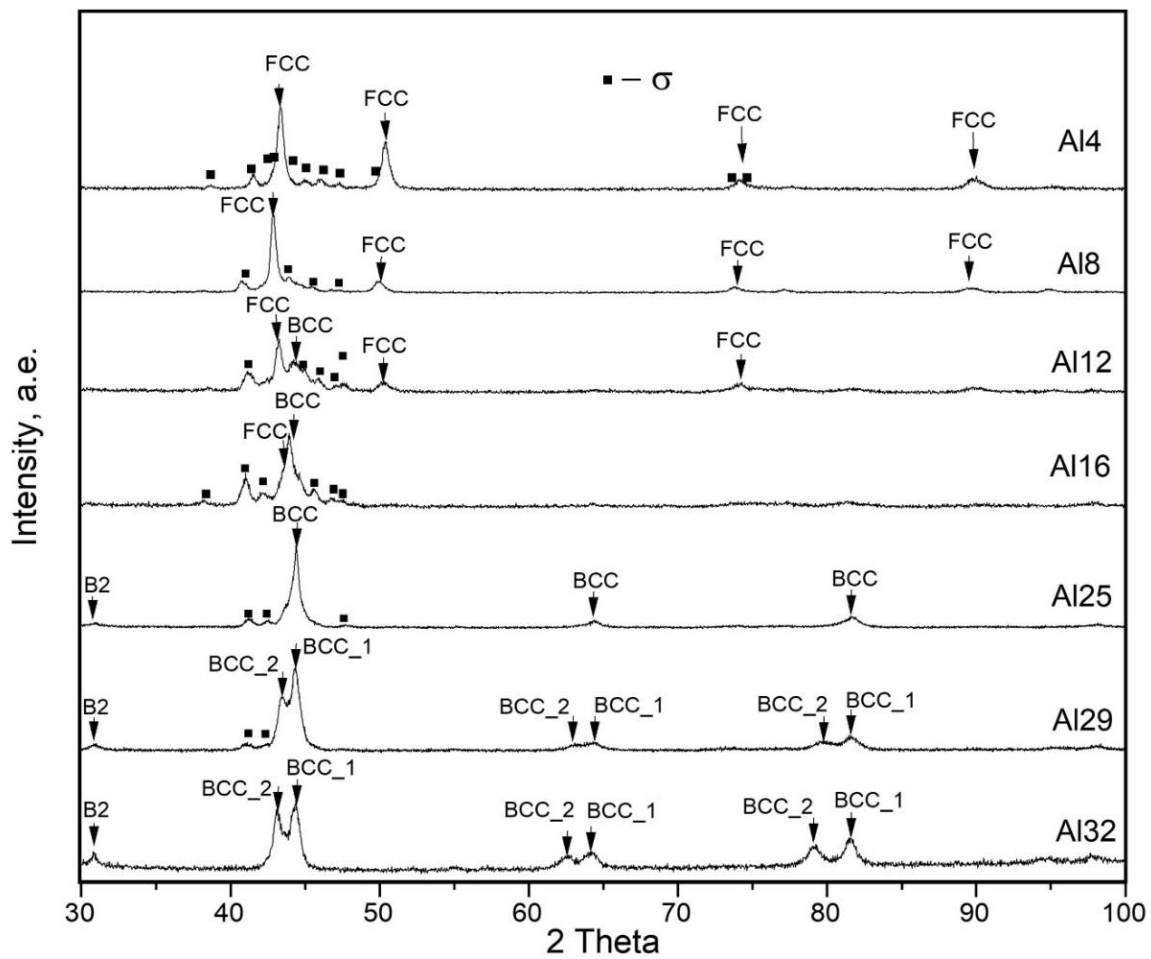


Figure 1. XRD patterns of the $\text{FeNiCoCrMo}_{0.5}\text{Al}_x$.

Table 2. Phase found by XRD.

Alloy	Phase/Lattice Parameter, Å
Al0	FCC/3.5960; σ -phase
Al4	FCC/3.6158; σ -phase
Al8	FCC/3.6248; BCC/2.8908; σ -phase
Al12	FCC/3.6151; BCC/2.8893; σ -phase
Al16	FCC/3.5885; BCC/2.8880; σ -phase
Al22	BCC(B2)/2.8823; σ -phase
Al25	BCC(B2)/2.8852; BCC_2/2.9098; σ -phase
Al29	BCC_1(B2)/2.8863; BCC_2/2.9434; σ -phase
Al32	BCC_1(B2)/2.8893; BCC_2/2.9636

3.2. Microstructure Observation

The microstructures and the element distribution for the alloys with an Al content of 4, 8, and 16 at.% are presented in Figures 2 and 3. The structural components of Al4 are primary FCC solid solution dendrites and interdendritic eutectic consisting of the FCC solid solution and σ -phase. When Al content is increased to 8 at.%, the microstructure changes considerably, and the structural components become much smaller. Instead of an eutectic on peripheries of the FCC dendrites, there is a layered structure consisting of two phases; one of these consists predominantly of Mo, Cr, and Fe, and another of Al and Ni.

According to the XRD, the results show the former is the σ -phase, and the latter is BCC(B2). Obviously, the layered structure formed as a result of FCC solid solution decomposition, the composition of which became unstable due to dendritic liquation. The length of the σ -phase did not exceed 2 μm , the thickness was 200 nm, and the size of the FCC dendrites was reduced by about 10 times compared to the previous alloy.

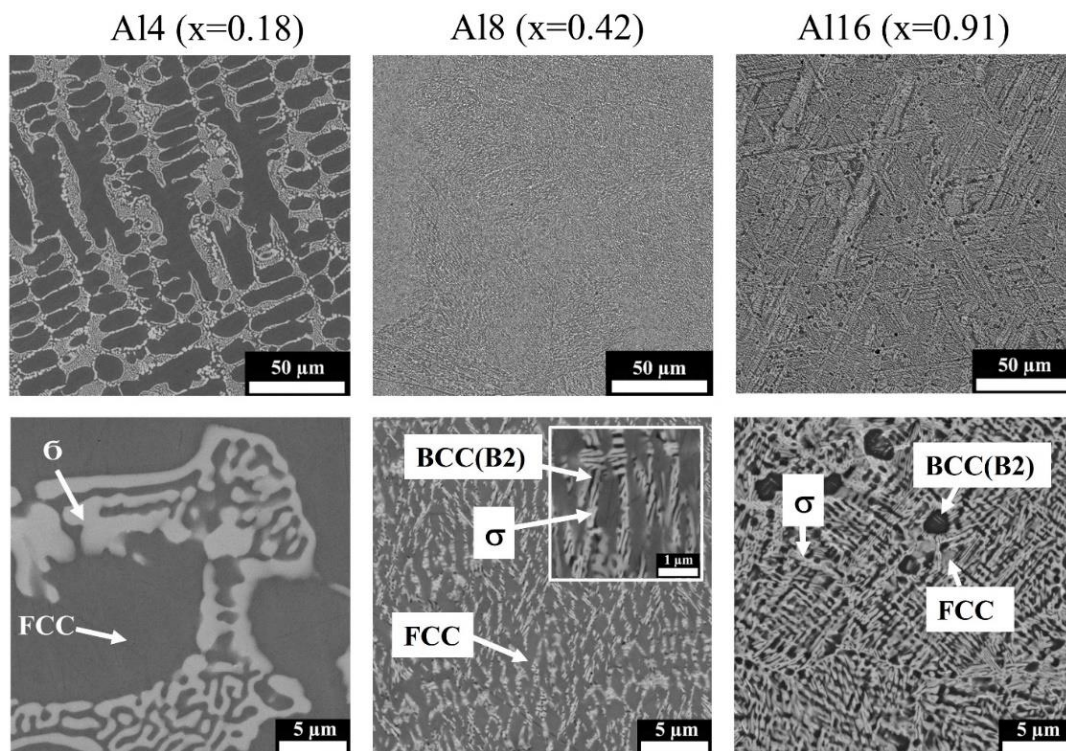


Figure 2. SEM microphotographs of the Al4, Al8, and Al16 alloys. σ -phase—the lightest, BCC(B2)—the darkest, and FCC—grey structural components.

Further increase in Al to 16 at.% considerably reduced the solution stability; one can see the σ and BCC(B2) phases, which is in agreement with the XRD observations, where only a small amount of FCC may be found. According to EDS, the σ -phase is enriched with Mo, Cr, and Fe; Al and Ni preferably form BCC(B2); Co is homogeneously distributed between both phases. The composition of the phases determined with EDS are presented in Table 3. It should be noted that the determined composition of the phases is not precise because of the small size of the phases and the limitations of the method.

The microstructures of the alloys with 22, 25, and 32 at.% Al and their elemental distributions are presented in Figures 4 and 5. All alloys had primary dendrites of BCC₁(B2), and its volume fraction increased with an increase in Al concentration. Inside the BCC₁(B2) dendrites, one can see thin coherent precipitates obviously caused by a decomposition of the solid solution. Interdendritic space in Al22 and Al25 is filled with a complex structure consisting of the σ -phase, BCC₁(B2), and BCC₂. However, in Al32, there were only traces of the sigma phase observed, and interdendritic space was predominantly filled with BCC₂ with spherical precipitates of BCC₁(B2).

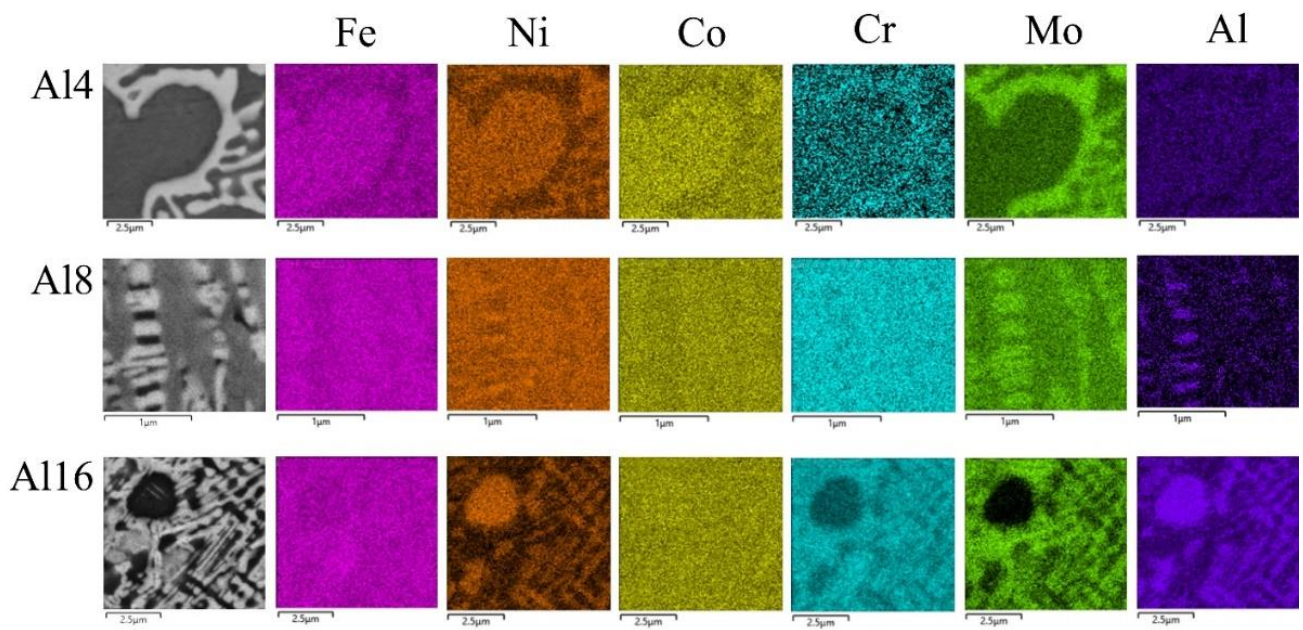


Figure 3. Elemental distribution in the Al4, Al18, and Al16 alloys.

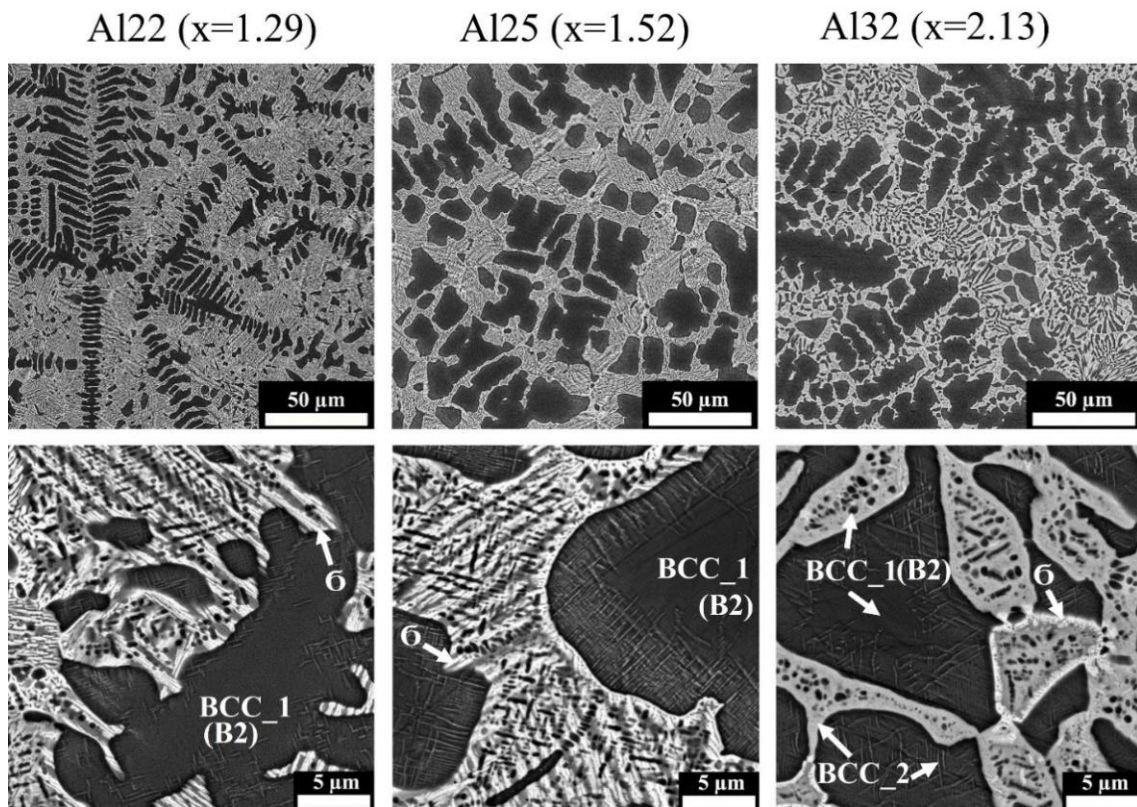
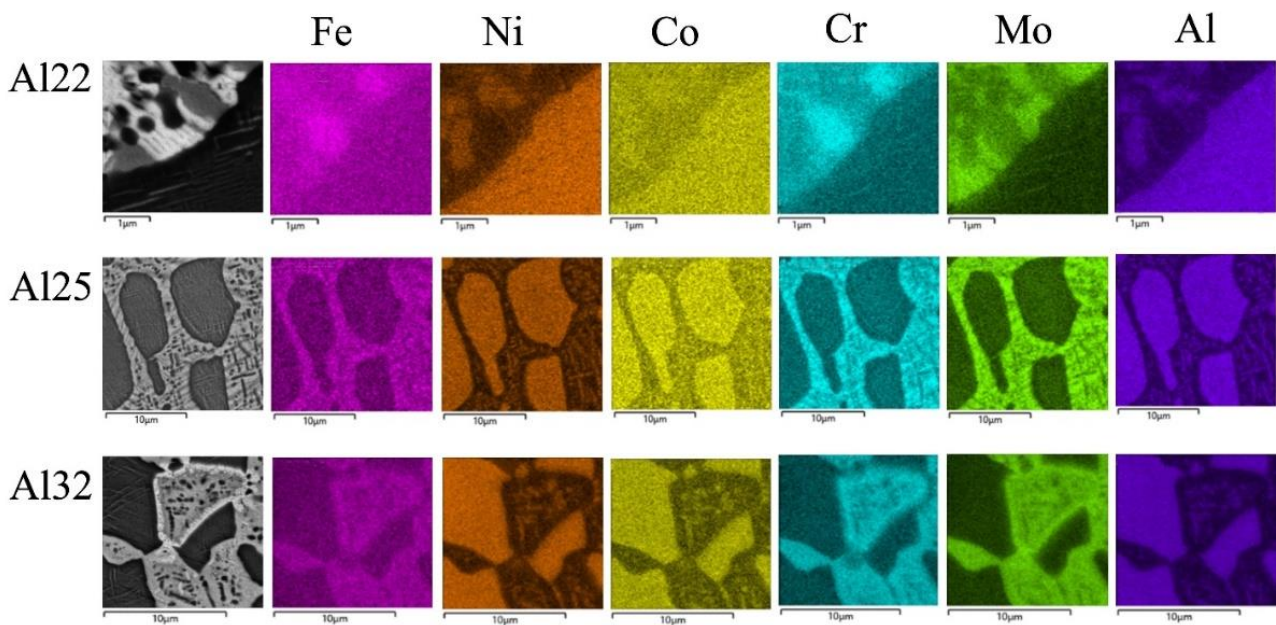


Figure 4. SEM microphotographs of the Al22, Al25, and Al32 alloys. σ -phase—the lightest, BCC_1(B2)—the darkest, and BCC_2—grey structural components.

Table 3. Composition of the phases determined with EDS.

Alloy	Phase	Atomic Concentration, %					
		Fe	Ni	Co	Cr	Mo	Al
Al4	FCC	22	22	22	21	9	4
	σ	18	14	18	25	21	4
Al8	FCC	21	22	21	19	8	8
	BCC(B2) *	18	24	20	17	7	14
Al12	σ *	19	17	19	23	15	6
	FCC	24	19	22	21	7	8
	BCC(B2)	17	25	19	16	5	18
Al16	σ	19	16	19	20	16	9
	BCC(B2)	15	28	17	14	4	21
Al22	σ	20	16	19	22	13	11
	BCC(B2)	13	24	18	10	3	31
Al25	Interdendritic	21	11	17	26	13	11
	BCC_1(B2)	14	20	18	13	5	30
Al29	Interdendritic	19	14	18	20	10	18
	BCC_1(B2)	14	20	18	12	5	32
Al32	Interdendritic	22	7	13	26	15	16
	BCC_1(B2)	13	19	17	9	5	37
	BCC_2	20	6	11	24	20	19

* Low accuracy due to the small size of the phase.

**Figure 5.** Elemental distribution in the Al22, Al25, and Al32 alloys.

4. Discussion

The volume fractions of the phases found in the investigated alloys were determined by two methods, XRD and SEM, and are presented in Figure 6.

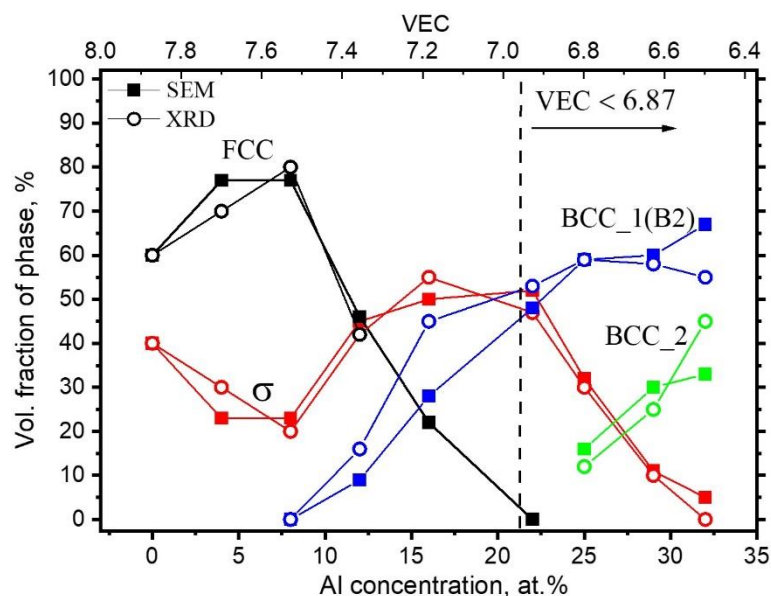


Figure 6. Volume fraction of phase in dependence of Al concentration determined by XRD (open circles) and SEM (squares).

At Al additions up to 8 at.%, a fraction of the FCC slightly increased; this may be explained by the dissolution of Al in the FCC solid solution. At higher Al concentration, the BCC phase occurs. Al is known as a BCC stabilizer, and an increase in Al content in Fe–Co–Ni–Cu–Cr–Mn–Al HEA leads to a change in the solid solution crystal lattice from FCC to BCC. This fact has been repeatedly demonstrated by different authors and is usually connected with valent electron concentration [27]. According to [27], at VEC less than 6.87, the FCC solid solution disappears and only the BCC structure forms, which is consistent with our observation for the Fe–Co–Ni–Mo–Cr–Al system (Figure 6). However, according to our observation, the formed BCC phase is an ordered NiAl-based B2 structure. Apart from the B2 phase, Al additions influence the amount of σ -phase. σ -phase was observed in HEA containing Cr, Fe, Co, and others after prolonged annealing [16,17,23,33] and in as-cast HEA alloys containing Mo and Fe [18,24,32]. Al does not participate in the σ -phase and suppresses its formation [34]. It is interesting that according to our observation, an increase in Al to 16–20 at.% led to a growth in σ -phase content (up to 50%) in spite of a decrease in the concentration of σ forming elements. At Al content over 22 at.%, the fraction of the σ -phase began to decrease and almost disappeared at 32 at.% Al. The decrease of σ -phase coincided with the formation of the second BCC_2 solid solution enriched with Mo, Cr, and Fe.

To explain this observation, a simplified scheme of the phase composition formation in dependence on Al content is proposed in Figure 7. σ -phase has AB stoichiometry, where A is an element of bigger atomic radius and less d electrons [34]. In the Fe–Co–Ni–Cr–Mo system, Cr and Mo are A elements, and Fe, Co, Ni–B elements. Despite Ni entering the σ -phase as a B element, it was reported as a destabilizer of the σ -phase in CrMnCoFeNi HEA [23]. In the composition of FeCoNiCrMo_{0.5} (0% Al) the ratio of A elements (Cr and Mo) to B elements (Fe, Co, and Ni) was 1:2. Because Ni is less prone to form the σ -phase compared to Fe and Co [35], it remains in excess and promotes FCC solid solution formation. This is consistent with [23], where it was reported that an excess of Ni results in FCC stabilization and σ -phase suppression.

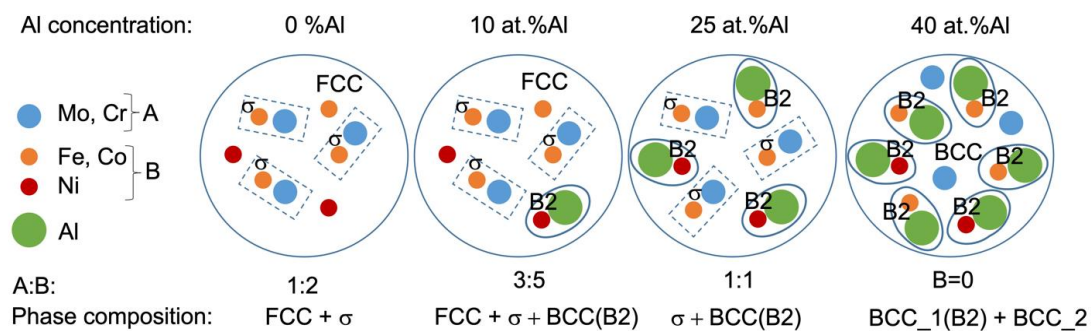


Figure 7. Atom distribution and the formation of the phase composition scheme. The indicated A:B ratio refers to the atoms, which are not bound with Al.

It can be suggested that in the multicomponent solution, each atom is most likely to be surrounded by other atoms, with which it has a higher negative enthalpy of mixing. Figure 8 presents the enthalpy of mixing for each pair of atoms in the system [37]. Based on this, Al attracts Ni first of all, leading to Al–Ni segregation. Thus, the more Al is added, the more Ni is bound to Al and, correspondingly, is removed from the solid solution. The removal of Ni from the FCC solid solution destabilizes it, leading to an additional σ -phase precipitation. It should be noted that the proposed scheme is only a simplified presentation, and it is obvious that not only do B elements (Ni, Co, and Fe) compose the FCC solid solution, but also that Cr and Mo have some solubility in it. Solubility of Cr and Mo in FCC was about 20 and 8 at.%; however, their solubility in B2 was only about 13 and 5 at.% correspondingly (Table.3). Therefore, an increase in the amount of B2 is followed by an increase in the amount of σ -phase. Further increase in Al concentration causes bonding not only with Ni, but also with Co and Fe, which occupy Ni positions in B2. This results in an excess of A elements (Mo, Cr) in the solution, which forms another BCC structure.

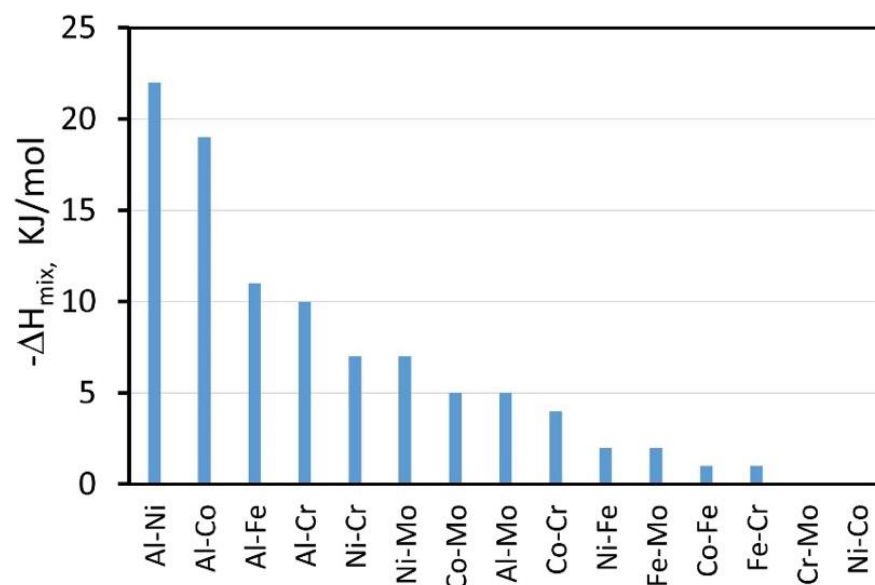


Figure 8. Negative enthalpy of mixing for the elements [37].

Figure 9 shows a change of interatomic distance in FCC, BCC_1(B2), and BCC_2 lattices depending on the alloy's concentration. An increase in Al content to 8 at.% caused an expansion of the FCC crystal lattice, taking into account an increase in the fraction of FCC (Figure 6), which proves that up to this concentration, Al dissolves in the FCC solid solution.

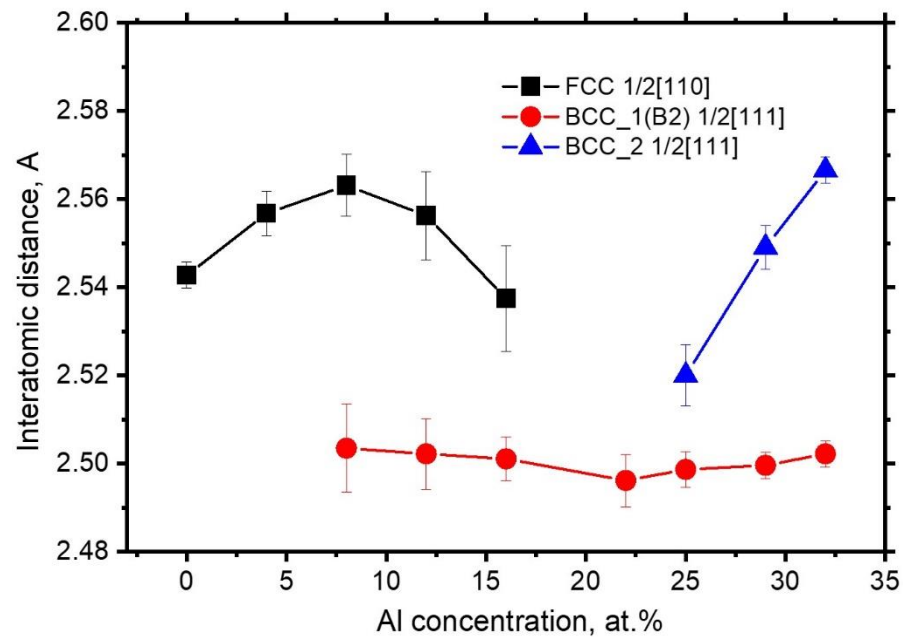


Figure 9. Change in the shortest interatomic distance in the crystal lattice of the solid solutions (FCC or BCC) in dependence of Al concentration in the alloy. The distance was calculated as $\frac{1}{2}$ (110) for FCC and as $\frac{1}{2}$ (111) for BCC lattices.

In the alloys with an Al concentration higher than 8 at.%, the FCC lattice parameter decreased, which showed a change in the FCC solid solution composition. As we proposed earlier, at this Al content, Ni leaves the solid solution after being attracted to Al. It is known that Ni has the smallest atom radius among the other elements of this system, and its removal from the solid solution should result in a growth of its lattice parameter, which contradicts with our observation. However, destabilization of the FCC solid solution due to Ni removal also leads to a removal of other elements with larger radii such as Mo, Cr, and Fe, which form the σ -phase, and the growth of the fraction of the σ -phase proves our assumption. On the other hand, a decrease in the FCC solid solution lattice parameter may be connected with the formation of a coherent BCC_1(B2) phase based on Al–Ni segregations, so the coherent boundaries may lead to elastic shrinkage of the FCC crystal structure.

The lattice parameter of the BCC_1(B2) phase was almost the same for all compositions, which may be a consequence of more rigid interatomic bonds or more constant composition compared to the FCC solid solution.

The lattice parameter of the second BCC_2 solid solution enriched with Cr and Mo strongly increased with an increase in Al concentration. As we suggested, Al bonds to σ -forming B elements, namely Ni, Co, and Fe into the BCC_1(B2) phase, and A elements with bigger atomic radius (Mo, Cr) remain in the BCC_2 solid solution, resulting in the increase in its lattice parameter.

5. Properties

Changes of the microhardness and density of the alloys in dependence on the Al content are shown in Figure 10. An increase in Al results in hardness growth; at an interval of 25–29 at.% Al, microhardness falls by 100 HV and then rises up again to 630 HV.

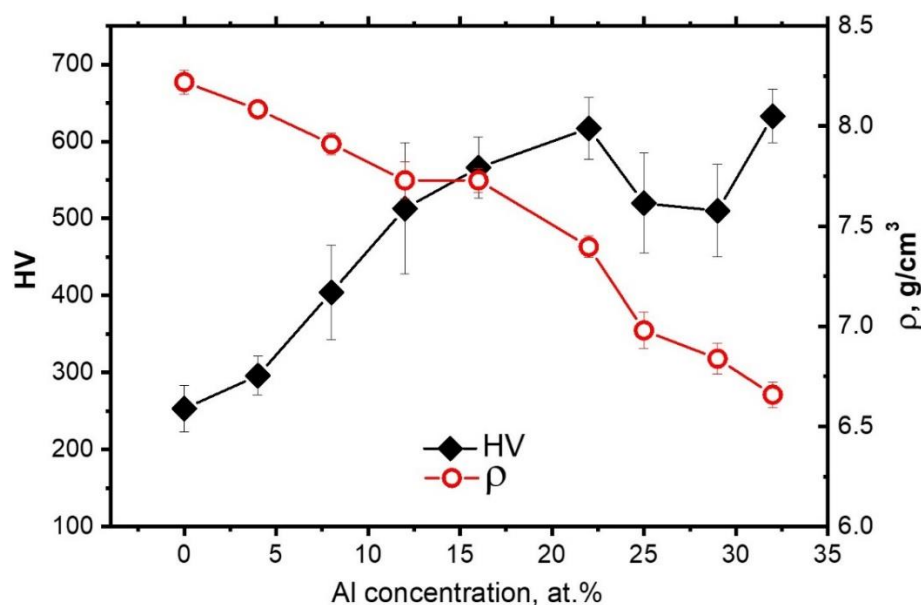


Figure 10. Microhardness and density of the alloys in dependence on Al concentration.

The microhardness rising with an Al concentration of up to 22 at.% is caused by both an increase in the amount of σ -phase and a formation of B2 instead of the soft FCC solid solution (Figure 3). The slight decline in the microhardness at the interval of 25–29 at.% may be associated with a decrease in the fraction of hard σ -phase. It is interesting that at 32 at.% Al, when the σ -phase almost disappeared, the microhardness leapt up by 100 HV, which may be explained by an increase in the amount of BCC₂ as well as its hardness due to a high concentration of Mo and Cr. As was said previously, an increase in Al (in interval of 25–32 at.%) led to an increase in Mo and Cr in the BCC₂ solid solution, which was confirmed by an increase in its lattice parameter (Figure 9). Thus, the composition of FeCoNiCrMo_{0.5}Al_{2.13} had the highest hardness of 630 HV and the lowest density of 6.65 g/cm³.

6. Conclusions

Multicomponent alloys of the FeCoNiCrMo_{0.5}Al_x system with x varying up to 2.13 were analyzed by XRD, SEM, EDS, and microhardness test. It was found that:

1. Al dissolves in an FeCoNiCrMo_{0.5} FCC solid solution up to 8 at.%. At higher concentrations, Al attracts Ni, removing it from the FCC solid solution and thereby destabilizing it. At an Al content of 22 at.% and higher, corresponding to $VEC \leq 6.87$, the FCC phase disappears. The Al and Ni formed the ordered BCC (B2) phase, in which Co and Fe also dissolve, occupying Ni positions.
2. Additions of Al to FeCoNiCrMo_{0.5} strongly influence the fraction of the σ -phase. Despite Al not participating in σ -phase formation, an increase in Al concentration to about 20 at.% led to a growth in the σ -phase fraction to 50%. The increase in σ -phase was caused by an increase in the amount of B2 instead of the FCC solid solution because the solubility of Mo and Cr in B2 was less than that in the FCC solution. A further increase in Al concentration led to an excess of Mo and Cr in the solution, which formed a disordered BCC solid solution. At an Al content of 32%, the alloy consisted of two BCC phases: a solid solution enriched with Cr and Mo and ordered B2 (Ni, Co)Al-based phase.
3. The rise in microhardness with an increase in Al concentration to 22 at.% was caused by both an increase in the amount of σ -phase and the formation of B2 instead of a soft FCC solid solution. In a composition with 32 at.% Al, when the σ -phase almost disappeared, the microhardness reached a maximum of 630 HV, which may be explained by both an increase in the fraction of disordered BCC enriched with Mo, and

by the increase in Mo concentration in it. Thus, the composition FeCoNiCrMo_{0.5}Al_{2.13} had the highest hardness of 630 HV and the lowest density of 6.65 g/cm³ among the considered compositions.

Author Contributions: A.S., S.S. and T.L.: investigation, visualization; V.A. and M.S.: methodology, SEM and XRD measurements; V.K.: validation; T.L., O.T. and V.K.: writing—original draft; O.T.: supervision. All authors have read and agreed to the published version of the manuscript.

Funding: The research was supported by the Ministry of Science and Higher Education of the Russian Federation (State Assignment for basic research 0784-2020-0022).

Institutional Review Board Statement: Not applicable.

Informed Consent Statement: Not applicable.

Data Availability Statement: The data presented in this study are available on request from the corresponding author.

Conflicts of Interest: The authors declare no conflict of interest.

References

1. Cantor, B.; Chang, I.T.H.; Knight, P.; Vincent, A.J.B. Microstructural development in equiatomic multicomponent alloys. *Mater. Sci. Eng. A* **2004**, *375–377*, 213–218. [[CrossRef](#)]
2. Yeh, J.W.; Chen, S.K.; Lin, S.J.; Gan, J.Y.; Chin, T.S.; Shun, T.T.; Tsau, C.H.; Chang, S.Y. Nanostructured high-entropy alloys with multiple principal elements: Novel alloy design concepts and outcomes. *Adv. Eng. Mater.* **2004**, *6*, 299–303. [[CrossRef](#)]
3. Zhang, Y.; Zhou, Y.J.; Lin, J.P.; Chen, G.L.; Liaw, P.K. Solid-solution phase formation rules for multi-component alloys. *Adv. Eng. Mater.* **2008**, *10*, 534–538. [[CrossRef](#)]
4. Yang, X.; Zhang, Y. Prediction of high-entropy stabilized solid-solution in multi-component alloys. *Mater Chem. Phys.* **2012**, *132*, 233–238. [[CrossRef](#)]
5. George, E.P.; Raabe, D.; Ritchie, R.O. High-entropy alloys. *Nat. Rev. Mater.* **2019**, *4*, 515–534. [[CrossRef](#)]
6. Yeh, J.W. Recent progress in high-entropy alloys. *Ann. Chim. Sci. Mater.* **2006**, *31*, 633–648. [[CrossRef](#)]
7. Zhang, Y.; Zuo, T.T.; Tang, Z.; Gao, M.C.; Dahmen, K.A.; Liaw, P.K.; Lu, Z.P. Microstructures and properties of high-entropy alloys. *Prog. Mater. Sci.* **2014**, *61*, 1–93. [[CrossRef](#)]
8. Pickering, E.J.; Jones, N.G. High-entropy alloys: A critical assessment of their founding principles and future prospects. *Int. Mater. Rev.* **2016**, *61*, 183–202. [[CrossRef](#)]
9. Singh, S.; Wanderka, N.; Murty, B.S.; Glatzel, U.; Banhart, J. Decomposition in multi-component AlCoCrCuFeNi high-entropy alloy. *Acta Mater.* **2011**, *59*, 182–190. [[CrossRef](#)]
10. López Ríos, M.; Socorro Perdomo, P.P.; Voiculescu, I. Effects of nickel content on the microstructure, microhardness and corrosion behavior of high-entropy AlCoCrFeNi_x alloys. *Sci. Rep.* **2020**, *10*, 21119. [[CrossRef](#)] [[PubMed](#)]
11. Shun, T.-T.; Hung, W.-J. Effects of Cr Content on Microstructure and Mechanical Properties of AlCoCr_xFeNi High-Entropy Alloy. *Adv. Mater. Sci. Eng.* **2018**, 5826467. [[CrossRef](#)]
12. Guo, L.; Xiao, D.; Wu, W.; Ni, S.; Song, M. Effect of Fe on Microstructure, Phase Evolution and Mechanical Properties of (AlCoCrFeNi)_{100-x}Fe_x High Entropy Alloys Processed by Spark Plasma Sintering. *Intermetallics* **2018**, *103*, 1–11. [[CrossRef](#)]
13. Reverte, E.; Cornide, J.; Lagos, M.A.; Campos, M.; Alvaredo, P. Microstructure Evolution in a Fast and Ultrafast Sintered Non-Equiatomic Al/Cu HEA. *Metals* **2021**, *11*, 848. [[CrossRef](#)]
14. Tong, C.-J.; Chen, Y.-L.; Yeh, J.-W.; Lin, S.-J.; Chen, S.-K.; Shun, T.-T.; Tsau, C.-H.; Chang, S.-Y. Microstructure characterization of Al_xCoCrCuFeNi high-entropy alloy system with multiprincipal elements. *Metall. Mater. Trans. A* **2005**, *36*, 881–893. [[CrossRef](#)]
15. Manzoni, A.; Daoud, H.; Völkl, R.; Glatzel, U.; Wanderka, N. Phase separation in equiatomic AlCoCrFeNi high-entropy alloy. *Ultramicroscopy* **2013**, *132*, 212–215. [[CrossRef](#)]
16. Stepanov, N.D.; Shaysultanov, D.G.; Ozerov, M.S.; Zherebtsov, S.V.; Salishchev, G.A. Second phase formation in the CoCrFeNiMn high entropy alloy after recrystallization annealing. *Mater. Lett.* **2016**, *185*, 1–4. [[CrossRef](#)]
17. Otto, F.; Dlouhý, A.; Pradeep, K.G.; Kubénová, M.; Raabe, D.; Eggeler, G.; George, E.P. Decomposition of the single-phase high-entropy alloy CrMnFeCoNi after prolonged anneals at intermediate temperatures. *Acta Mater.* **2016**, *112*, 40–52. [[CrossRef](#)]
18. Juan, C.C.; Hsu, C.Y.; Tsai, C.W.; Wang, W.R.; Sheu, T.S.; Yeh, J.W.; Chen, S.K. On microstructure and mechanical performance of AlCoCrFeMo_{0.5}Ni_x high-entropy alloys. *Intermetallics* **2013**, *32*, 401–407. [[CrossRef](#)]
19. Li, C.; Ma, Y.; Hao, J.; Yan, Y.; Wang, Q.; Dong, C.; Liaw, P.K. Microstructures and mechanical properties of body-centered-cubic (Al, Ti)_{0.7}(Ni, Co, Fe, Cr)₅ high entropy alloys with coherent B2/L2₁ nanoprecipitation. *Mater. Sci. Eng. A* **2018**, *737*, 286–296. [[CrossRef](#)]
20. Ma, Y.; Jiang, B.; Li, C.; Wang, Q.; Dong, C.; Liaw, P.K.; Xu, F.; Sun, L. The BCC/B2 Morphologies in Al_xNiCoFeCr High-Entropy Alloys. *Metals* **2017**, *7*, 57. [[CrossRef](#)]

21. Detrois, M.; Antonov, S.; Tin, S. Phase Stability and Thermodynamic Database Validation in a Set of Nonequiatomic Al-Co-Cr-Fe-Nb-Ni High-Entropy Alloys. *Intermetallics* **2019**, *104*, 103–112. [[CrossRef](#)]
22. Pickering, E.J.; Stone, H.J.; Jones, N.G. Fine-scale precipitation in the high-entropy alloy Al_{0.5}CrFeCoNiCu. *Mater. Sci. Eng. A* **2015**, *645*, 65–71. [[CrossRef](#)]
23. Christofidou, K.A.; McAuliffe, T.P.; Mignanelli, P.M.; Stone, H.J.; Jones, N.G. On the prediction and the formation of the sigma phase in CrMnCoFeNi_x high entropy alloys. *J. Alloys Compd.* **2019**, *770*, 285–293. [[CrossRef](#)]
24. Mukarram, M.; Munir, M.A.; Mujahid, M.; Yaqoob, K. Systematic Development of Eutectic High Entropy Alloys by Thermodynamic Modeling and Experimentation: An Example of the CoCrFeNi-Mo System. *Metals* **2021**, *11*, 1484. [[CrossRef](#)]
25. Tokarewicz, M.; Grądzka-Dahlke, M. Review of Recent Research on AlCoCrFeNi High-Entropy Alloy. *Metals* **2021**, *11*, 1302. [[CrossRef](#)]
26. Troparevsky, M.C.; Morris, J.; Daene, M.; Wang, Y.; Lupini, A.; Stocks, G.M. Beyond Atomic Sizes and Hume-Rothery Rules: Understanding and Predicting High-Entropy Alloys. *JOM* **2015**, *67*, 2350–2363. [[CrossRef](#)]
27. Guo, S.; Ng, C.; Lu, J.; Liu, C.T. Effect of valence electron concentration on stability of fcc or bcc phase in high entropy alloys. *J. Appl. Phys.* **2011**, *109*, 103505. [[CrossRef](#)]
28. Ogura, M.; Fukushima, T.; Zeller, R.; Dederichs, P.H. Structure of the High-Entropy Alloy Al_xCrFeCoNi: Fcc versus Bcc. *J. Alloys Compd.* **2017**, *715*, 454–459. [[CrossRef](#)]
29. Frommeyer, G.; Rablbauer, G. High temperature resistant intermetallic NiAl-based alloys with refractory metals Cr, Mo, Re. *Mater. Res. Soc. Symp. Proc.* **2003**, *753*, BB4.6.1–BB4.6.15. [[CrossRef](#)]
30. Ma, S.G.; Zhang, Y. Effect of Nb Addition on the Microstructure and Properties of AlCoCrFeNi High-Entropy Alloy. *Mater. Sci. Eng. A* **2012**, *532*, 480–486. [[CrossRef](#)]
31. Dong, Y.; Zhou, K.; Lu, Y.; Gao, X.; Wang, T.; Li, T. Effect of Vanadium Addition on the Microstructure and Properties of AlCoCrFeNi High Entropy Alloy. *Mater. Des.* **2014**, *57*, 67–72. [[CrossRef](#)]
32. Shun, T.T.; Chang, L.Y.; Shiu, M.H. Microstructure and mechanical properties of multiprincipal component CoCrFeNiMo_x alloys. *Mater. Charact.* **2012**, *70*, 63–67. [[CrossRef](#)]
33. Pickering, E.J.; Muñoz-Moreno, R.; Stone, H.J.; Jones, N.G. Precipitation in the equiatomic high-entropy alloy CrMnFeCoNi. *Scr. Mater.* **2016**, *113*, 106–109. [[CrossRef](#)]
34. Hall, E.O.; Algie, S.H. The sigma phase. *Int. Mater. Rev.* **1966**, *11*, 61–88. [[CrossRef](#)]
35. Lee, C.; Lee, Y.; Lee, C.; Hong, S. Precipitation behavior of the sigma phase with Ni and Mn content variations in superaustenitic stainless steel weld metal. *Mater. Charact.* **2018**, *144*, 148–154. [[CrossRef](#)]
36. Nelson, J.B.; Riley, D.P. An Experimental Investigation of Extrapolation Methods in the Derivation of Accurate Unit Cell Dimensions of Crystals. *Proc. Phys. Soc.* **1945**, *57*, 160–177. [[CrossRef](#)]
37. Takeuchi, A.; Inoue, A. Classification of Bulk Metallic Glasses by Atomic Size Difference, Heat of Mixing and Period of Constituent Elements and Its Application to Characterization of the Main Alloying Element. *Mater. Trans.* **2005**, *46*, 2817–2829. [[CrossRef](#)]